

Preparation of MWCNTs/Cr₂O₃-NiO Nanocomposite for Adsorption and Photocatalytic Removal of Bismarck Brown G Dye from Aqueous Solution

Emman Jassim Mohammad, Mohanad Mousa Kareem, and Abbas Jasim Atiyah Lafta*

Department of Chemistry, College of Science, University of Babylon, Hilla 51002, Iraq

* Corresponding author:

email: abbaslafta2009@yahoo.com

Received: February 6, 2019

Accepted: April 28, 2019

DOI: 10.22146/ijc.43429

Abstract: This work describes the synthesis of nanocomposites of multiwall carbon nanotubes (MWCNTs) with co-oxide nanocomposite (MWCNTs)/MO. These nanocomposites were prepared using a simple evaporation and drying process. The obtained composites were characterized using X-Ray diffraction (XRD), Atomic force microscopy (AFM), Fourier Transform Infrared Spectroscopy (FTIR), and scanning electron microscopy (SEM). The activity of the prepared composites was investigated by following the removal of Bismarck brown G dye (BBG) from aqueous solution via adsorption processes and photocatalytic reactions. Different reaction parameters were performed, such as the effect of dosage of the used nanocomposite, pH value, and effect of temperature. In addition, adsorption isotherms and reaction kinetics were investigated. The efficiency of photocatalytic dye removal over the prepared composites was 99.9% after one hour of reaction at the optimal conditions, which were mass dosage (0.03 g), pH (5), and temperature (303 K). The adsorption isotherm data were fitted with Langmuir isotherm, and the kinetic data were fitted with the pseudo-second-order kinetic model.

Keywords: dyes removal; Bismarck brown G; carbon nanotubes; nanocomposite

■ INTRODUCTION

In 1991, Sumit discovered an inert carbonaceous compound that has very important and powerful properties that are called carbon nanotubes (CNTs) [1]. The first explored was of the type of multi walled carbon nanotubes (MWCNTs). This is a metallic compound and results from rolling single walled carbon nanotubes many times like (Russian doll) [2]. MWCNTs are bigger objects with diameters in the range of 1.4–100 nm and length from 1 to several μm . It has a tensile strength about 100 times stronger as compared to steel and excellent thermal and electrical conductivities [3]. CNTs have a wide range of application due to its chemical, mechanical, electronic, and optical properties [4]. There are several types of carbon nanotubes likes single walled carbon nanotube (SWCNT), which has been discovered in 1993 by Iijima [5]. SWCNTs metallic or semiconductor depends on its diameter and chirality [6]. SWCNTs can be existing in three forms, Zigzag, Armchair, and chiral this depends on the way how to arrange the graphene into a cylinder. SWCNT have a diameter from 0.4 to 2.0 nm and length in

the range of 20–1000 nm [7]. Different methods are used to synthesize CNT/MOs nanocomposites, such as thermal decomposition of metal oxides precursor, chemical vapor deposition (CVD) synthesis route, hydrothermal crystallization, chemical precipitation, high-intensity ultrasonic radiation method and spontaneous formation of metal oxide nanoparticles on CNTs [8-11].

Activation (functionalization) of CNTs can be performed using various methods, including chemical, and physical methods. Chemical methods (covalent functionalization) consist of introducing functional groups on the surface of CNTs using oxidizing agents such as nitric acid, sulfuric acid, potassium permanganate or a mixture of sulfuric acid and nitric acid, hydrogen peroxide in the presence of nitric acid with oxygen-or microwave energy and water. Physical methods (Non-covalent functionalization) include using different adsorption forces, such as hydrogen bonds, Van der Waals force, electrostatic force, and π -stacking interactions. Non-covalent surface

functionalization frequently introduces little defects to the graphitic structure and does not destroy the conjugated system of the CNT sidewalls, which is important to maintain the pristine structure and properties of CNTs [12-13].

Before synthesizing the CNT/MO nanocomposite, CNTs should be functionalized [14-18]. Functionalization of CNTs plays an important step to make the CNTs soluble in water and have chemical functional groups on the surface of nanotubes, including alcoholic, carboxylic, aldehydic, ketonic, and esteric oxygenated functional groups [19]. Another activation method uses mechanical methods, which involving high shear mixing, grinding and impact mixing, or ultrasonication to open the agglomeration. These methods can separate nanotubes, but it is ineffective approaches due to breaking up of some nanotubes [20-21].

CNT, when combining with metal oxides (MOs), can produce new composites materials with new interesting properties. In addition, combining these materials in nanocomposite scales can reduce some of the disadvantages properties. As a result, the nanocomposites have large applications in comparison with the separated nanoparticles because CNTs act as a carrier to stabilize the nanoparticles. CNT/MOs nanocomposites have high specific surface areas with active surfaces for physical adsorption and chemical adsorption. In this context, different parameters need to be optimized, such as the initial concentration of the organic pollutant, contact time, adsorbent dosage, pH of reaction mixture and effect of the presence of other cations and anions in reaction mixture [22-23]. In the last few decades, high levels of pollution emerged as a result of the industrial revolution and a dramatic increase in population. Many factories over the world and especially from textile factories and dyeing factories discharge their waste directly into the environment without and pretreatment. This can lead to polluting each of rivers, soil, and even groundwaters. So, many types of research were directed to find proper approaches in order to reduce the level of pollutions, and among different types of pollution, pollution with textile dyes was an important type of pollution. In this context, many methods were applied to treat pollution of water

with these dyes. Among these approaches, adsorption and photocatalytic dye treatment were undertaken as these routes can be performed and showed good removal efficiencies of polluted dyes from industrial water.

The present study describes the preparation of nanocomposites materials of functionalized multi-walled carbon nanotubes and Cr₂O₃-NiO co-oxide in different ratios. Then the activity of these prepared composites materials (MWCNTs/Cr₂O₃-NiO) would be investigated by following removal of Bismarck brown G dye (BBG) by adsorption and photocatalytic reaction over these prepared nanocomposites.

■ EXPERIMENTAL SECTION

Materials

MWCNTs were purchased from Nanoshel—the USA with a diameter of 13–18 nm, length in the range of 1–12 μm, and purity 99%. Sulfuric acid and Nitric acid from (BDH), Bismarck brown G that has a molecular formula (C₂₁H₂₄N₈·2HCl) was obtained from (Al-Hilla Textile Factory-Iraq).

Instrumentation

Atomic force microscope and Scanning Electron Microscope (FESEM) was used to investigate the surface morphology. Crystal structure of the prepared nanocomposite was investigated using powder X-Ray analysis, Phillips X-Ray diffraction with CuKα radiation (1.542 Å, 40 KV, 30 MA), in the 2θ range, 10–80 degrees. XRD6000, Shimadzu, Japan. Functional groups on the surface of the prepared composite were investigated using Fourier Transform spectroscopy (FTIR), 8400S Shimadzu Japan. FTIR spectra were recorded in the range of 400–4000 cm⁻¹, materials were mixed with powder of KBr in a ratio of 1.20. The topography of the surface of the prepared materials was investigated using an Atomic Force Microscope SPM-AA3000. Atomic Force Microscope/Contact Mode Angstrom Advanced Inc., 2005, USA. General morphological features and surface morphology of the prepared nanocomposites were investigated using SEM instrument JEOL JSM-6700F instrument (Germany). In addition, it was utilized in the calculation of the average particle size.

The EDX was used to measure the percentage of atomic ratio of MO, and functional group on the surface of the nanocomposites.

Procedure

Functionalization of MWCNTs

In order to convert MWCNTs from its inactive nature into the active form, 1 g. of raw MWCNTs was taken and added to a mixture of $\text{HNO}_3:\text{H}_2\text{SO}_4$ (1:3). The obtained mixture was then heated at 353 K and sonicated for 8 h. Then the obtained solution was filtered out by filter funnel borosilicate 3.3 (par. 3). The resulting suspension washed several times with distilled water until its pH reaching a value of 7. Then F-MWCNTs were dried at 373 K for 10 h [24]. Fig. 1 shows the preparation of MWCNTs/MO.

Synthesis of the nanocomposite

The nanocomposite of (MWCNTs/ $\text{Cr}_2\text{O}_3\text{-NiO}$) was prepared using a simple evaporation and drying process [25]. This composite was prepared by adding MWCNTs to MO ($\text{MO} = \text{Cr}_2\text{O}_3\text{-NiO}$) in the mass ratio of 1:0.5 g., then MWCNTs were dispersed into 100 mL, and MO was added into 20 mL of distilled water. The MWCNTs mixture was stirred for 35 min, and MO mixture was stirred for 20 min. Then MWCNTs mixture was added into MO suspension along with stirring and heating to 353 K to evaporate water from the obtained mixture. After that, the obtained composite was dried overnight in an oven at 373 K. Fig. 2 shows the schematic diagram of the experimental procedure for the preparation of MWCNTs/MO nanocomposite by using simple evaporation and drying process.

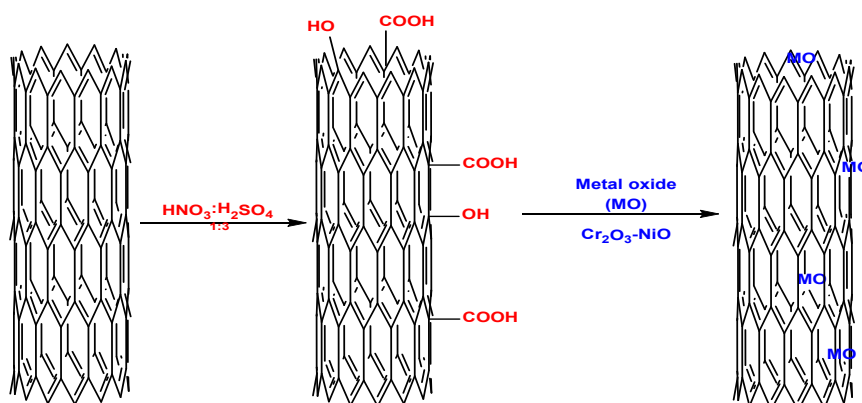


Fig 1. Functionalization and synthesis of carbon nanotubes/metal oxide (CNT/MO) composites

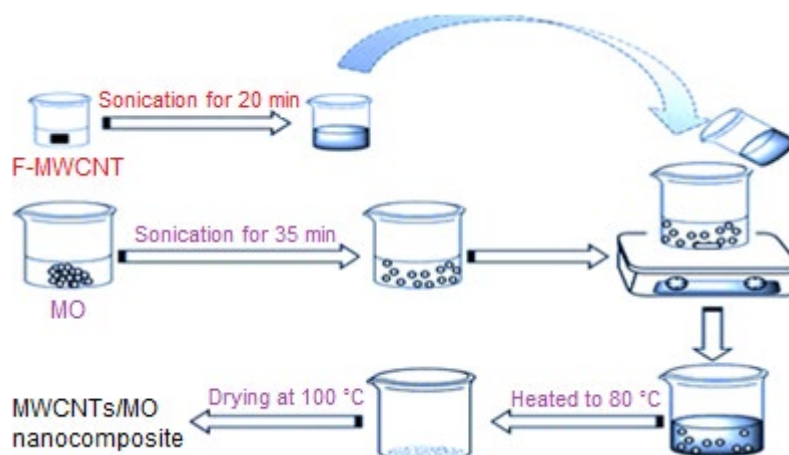


Fig 2. Schematic diagram of the experimental procedure for the preparation of MWCNTs/ $\text{Cr}_2\text{O}_3\text{-NiO}$ nanocomposite by using simple evaporation and drying process

Photocatalytic removal of BBG

All experiments were performed by adding nanocomposite material into a reaction mixture, and each reaction patch consists of 30 mL, 50 ppm of the BBG dye aqueous solution. In all experiments, reactions were initiated by the stirring reaction mixture in the dark for ten minutes. Then the reaction was initiated by flushing UV radiation from a middle-pressure mercury lamp. The photocatalytic processes were performed using a mercury lamp (Philips Holland (250 W)) without cover glass as a source of UV radiation, magnetic stirrer, hot plate, and photoreaction cell which was made from Pyrex glass with quartz windows. Periodically, the reaction mixture was withdrawn at every 10 min for 1 h and centrifuged carefully. Then the absorbance's of the supernatant liquids was recorded at 460 nm using UV-Visible spectrophotometer (Shimadzu1100A). The efficiency of photocatalytic dye removal was calculated using the following equation:

$$\% \text{ Photodegradation efficiency} = \frac{A_0 - A_t}{A_0} \times 100 \quad (1)$$

where the A_0 , A_t is the initial, and the final absorbance of the used dye, respectively.

Study effect of pH, temperature and nanocomposite dosages on dye removal

In order to obtain optimum reaction conditions that can achieve high removal efficiency for dye over the prepared nanocomposites materials, a series of experiments were carried out to determine the optimum weight, pH, and temperature of the reaction mixture. To obtain an optimum used mass of the prepared composite (MWCNT/Cr₂O₃-NiO), a dye solution with a concentration of 50 ppm was suspended with graduated masses of materials nanocomposite (0.006, 0.01, 0.03, 0.05 g). The reaction was then initiated by irradiation with UV light at room temperature. From this study, the optimum mass of nanocomposite can be evaluated. Then the same arrangement would be followed to evaluate the optimum temperature by setting a series of experiments using an optimum mass that obtained from the previous study and by varying experiments at different temperatures (283, 288, 293, 298, 303, and 308 K). Then optimum pH would be investigated by performing a series of experiments with

different pH values (pH = 2, 4, 5, and 9). The pH values were adjusted at the desired level using 0.01 M NaOH or 1.0 M HCl solutions. These experiments were carried out using the same above arrangements under irradiation for 60 min. The absorbance for the above solutions was measured at $\lambda_{\text{max}} = 460$ nm, and the efficiency of photocatalytic removal of this dye was calculated using the relation that was mentioned in Eq. 1.

Adsorption ability of the prepared catalyst

The adsorption ability of the prepared nanocomposites materials was investigated using 50 ppm of BBG dye solution in 100 mL. These samples were stirred at room temperature without light using different masses of the nanocomposite (0.006, 0.01, 0.03, 0.05 g). In each case, the reaction mixture was stirred continuously at room temperature under normal atmospheric conditions. Then periodically, 1 mL of the reaction mixture was withdrawn and centrifuged, and the absorbance of the obtained supernatant liquid was recorded at 460 nm. Then removal efficiency was evaluated using the above relation in Eq. 1.

RESULTS AND DISCUSSION

Characteristics of Nanocomposites

XRD patterns of F-MWCNTs are shown in Fig. 3 and presented in Table 1. These patterns showed unfavorable amorphous carbon materials, a strong intense peak at $2\theta = 24.6^\circ$, 26° , and a low intense peak at $2\theta = 43.5^\circ$. These peaks are corresponding to the (002) and (100) reflections, respectively. In comparison with that for MWCNTs, $2\theta = 25.2^\circ$ and $2\theta = 44.0^\circ$, these peaks showed a downhill shift which refers to a rise in the sp^2

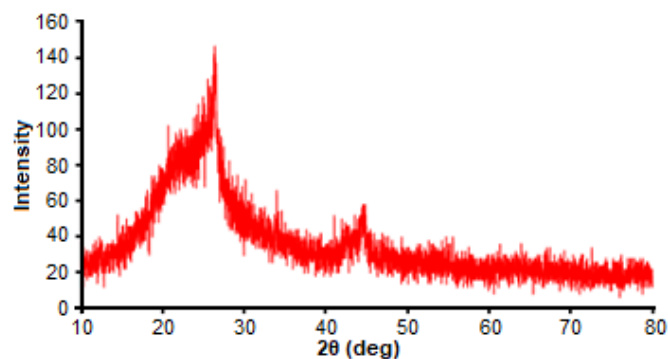
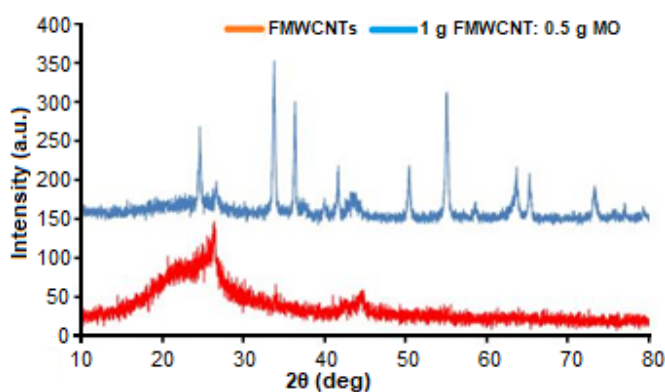


Fig 3. XRD pattern for F-MWCNT

Table 1. XRD patterns features of the MWCNTs and F-MWCNTs samples

Sample	2 θ (deg)		
MWCNT	25.2		44.0
F-MWCNT	24.6	26.0	33.9

**Fig 4.** XRD patterns of nanocomposite MWCNTs/Cr₂O₃-NiO**Table 2.** Values of angles diffraction 2 θ , and particle size of nanocomposite/MWCNTs/Cr₂O₃-NiO

Sample	2 θ (deg)	Crystalline size (nm) Average
Nanocomposite	24.6557	30.83
MOMWCNTs: 0.5 1 g	26.6581	
	33.7712	
	36.3478	
	37.1410	
	41.6543	
	43.3950	
	50.4008	
	55.0413	
	58.5748	
	63.6123	
	65.2709	
73.2404		
77.0343		
79.2987		

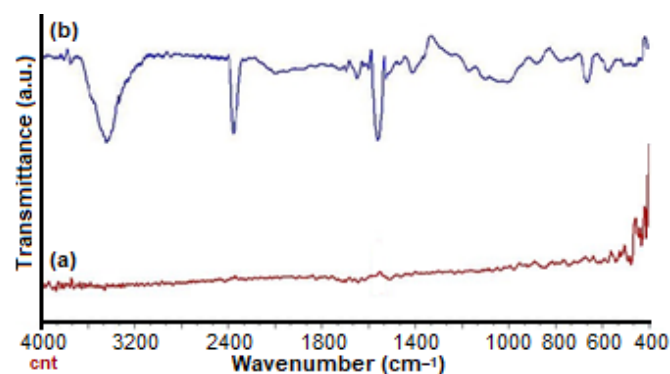
C=C layer spacing and suggests that crystalline did not miss due to oxidative acid process. In this context, XRD patterns can be used to explain a relation between the degree of carbon nanotube and intensity of the oxidation MWCNTs (002) peak [26]. Table 1 shows a comparison of the XRD spectra features of the MWCNTs and F-MWCNTs samples.

X-Rays Diffraction of MWCNTs/Cr₂O₃-NiO Nanocomposite (XRD)

XRD patterns of MWCNTs/Cr₂O₃-NiO nanocomposites 1:0.5 g are shown in Fig. 4. XRD patterns of the nanocomposite are extremely similar to that of Cr₂O₃-NiO with the appearance of peaks at 24.6, 26.5, 43.3° for MWCNTs. The increase of FMWCNT ratio causes gradually decrease in the crystallite size of the MWCNTs/MO, and it becomes broader and more intense with an increase of the ratio of MWCNTs in the nanocomposite [27-28]. This observation can be related to the increase of the surface area of the composites with a reduction in the average particle size in comparison with the particle size of neat Cr₂O₃-NiO (36.18 nm). This probably arises from the high specific surface area of CNTs.

Fourier Transform Infrared Spectroscopy of MWCNTs and F-MWCNTs (FTIR)

Fourier Transform Infrared spectral data of MWCNTs and F-MWCNTs are presented in Fig. 5(a) and (b) for MWCNTs and F-MWCNTs respectively in the range of 400–4000 cm⁻¹. FTIR spectra of MWCNTs show a peak around 1680–1640 cm⁻¹, this peak is assigned to –C=C– of alkenes and that around 1500–1400 cm⁻¹ is assigned to C–C stretching in the aromatic ring [29-31]. The peak around 2400 cm⁻¹ is assigned to the compensation of carbon dioxide and water at the surface. The FTIR spectra of F-MWCNT show a peak around 1760–1690 cm⁻¹ and this peak is assigned to C=O stretching vibration of the carboxyl group. The peak around 3500–3200 cm⁻¹ is assigned to the OH vibration

**Fig 5.** FTIR spectra of the MWCNTs (a), and FTIR spectra of the F-MWCNTs (b)

mode of O-MWCNTs. The peak around $1320\text{--}1000\text{ cm}^{-1}$ is assigned to stretching vibration of C–O group in F-MWCNTs [32]. The peak around $2900\text{--}3100\text{ cm}^{-1}$ can be attributed to the vibration of the C–H bond.

Fourier Transform Infrared Spectroscopy of MWCNTs/Cr₂O₃-NiO Nanocomposite

The FTIR spectra of the MWCNTs/MO nanocomposites are shown in Fig. 6. From these spectra, three obvious peaks correspond to the (MO) bonds around $432\text{--}619\text{ cm}^{-1}$, which belong to metal-oxygen bond and the –OH bond around $1639\text{--}1681\text{ cm}^{-1}$, and H bond at 3383 cm^{-1} . This is possibly arising from the intermolecular interaction at the surface of MO. However, the three absorption peaks of the MWCNTs/MO nanocomposite shifted towards higher wavelengths due to stronger interactions between the polar groups on the MO and functional groups at the surface of MWCNTs [33].

Atomic Force Microscopy (AFM) of the Prepared Nanocomposite

From the obtained results of AFM images, the average particle diameter of the prepared Cr₂O₃-NiO was around 74.65 nm at a calcination temperature of 773 K. This means that co-precipitation method effective to prepare catalysts in nanoscale and used in different industrial and environmental applications. Also, the

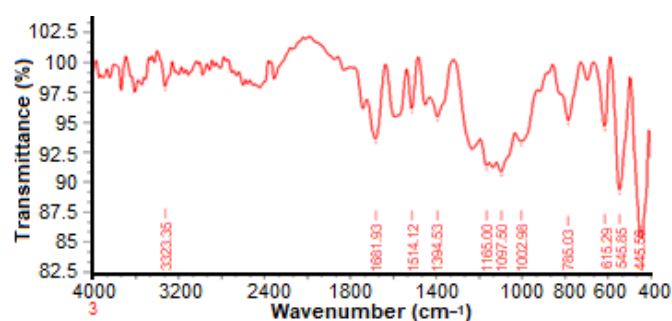


Fig 6. FTIR spectra of the MWCNTs/Cr₂O₃-NiO nanocomposite (1:0.5)

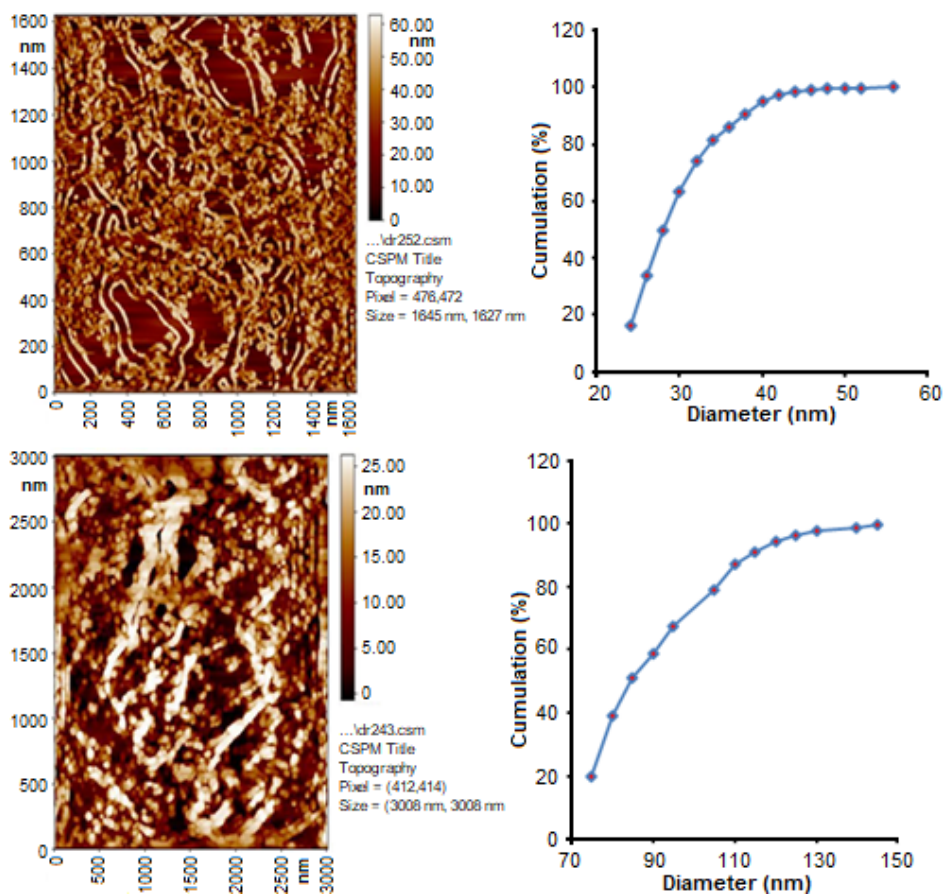


Fig 7. AFM images of nanocomposite F-MWCNTs/ Cr₂O₃-NiO (1:0.5) g

average particle diameter of the F-MWCNTs was 29.24 nm due to having a high surface area with small average particle size. The composite material showed an average particle diameter around 88.52 nm. This increment in particle size for a composite is probably due to the aggregation of particles that occurs at the surface of the prepared nanocomposite materials. AFM images of nanocomposite F-MWCNTs/Cr₂O₃-NiO (1:0.5) g are shown in Fig. 7.

Scanning Electron Microscope (SEM) of the Prepared Nanocomposites

The morphology of the prepared FMWCNT and MWCNTs/Cr₂O₃-NiO nanocomposite materials were investigated using SEM. This technique also was utilized to evaluate the average particle sizes. Fig. 8 and 9 show SEM images and ED's analysis for the MWCNTs, and

MWCNTs/Cr₂O₃-NiO nanocomposite.

Fig. 8 shows SEM images of F-MWCNTs; from these images, it can be noted that the morphology shows the presence of smaller aggregates and tangled clusters after functionalization. The spectra of SEM-EDX of the F-MWCNTs show two important peaks corresponding to C and O result from the oxidation process with other impurities. Fig. 9 shows SEM images of the morphology F-MWCNTs/MO nanocomposites. The SEM images showed that the MWCNTs are homogeneously distributed throughout the MO matrix with an obvious agglomeration of the MO particles. SEM-EDX used for elemental analysis as shown in Fig. 9 shows that the nanocomposite elements F-MWCNTs/MO exhibited several peaks, which related to Ni, Cr, C, and O with few impurities in the prepared composite [34].

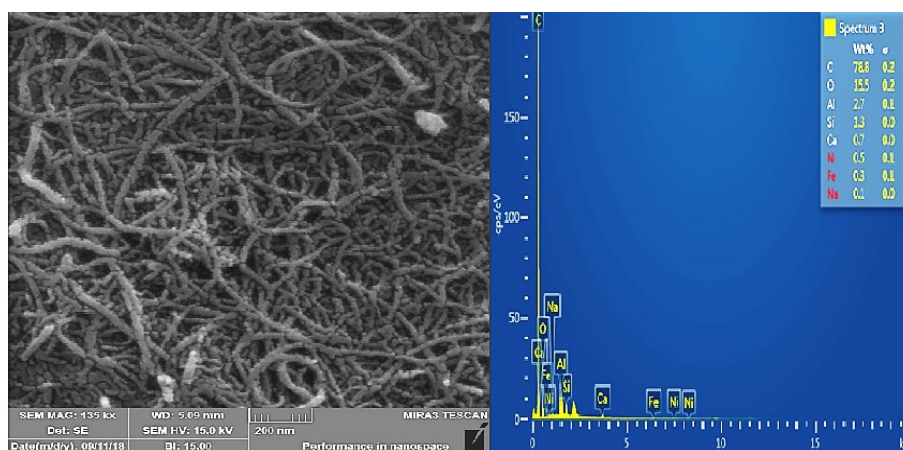


Fig 8. SEM images and EDS analysis of the prepared F-MWCNTs

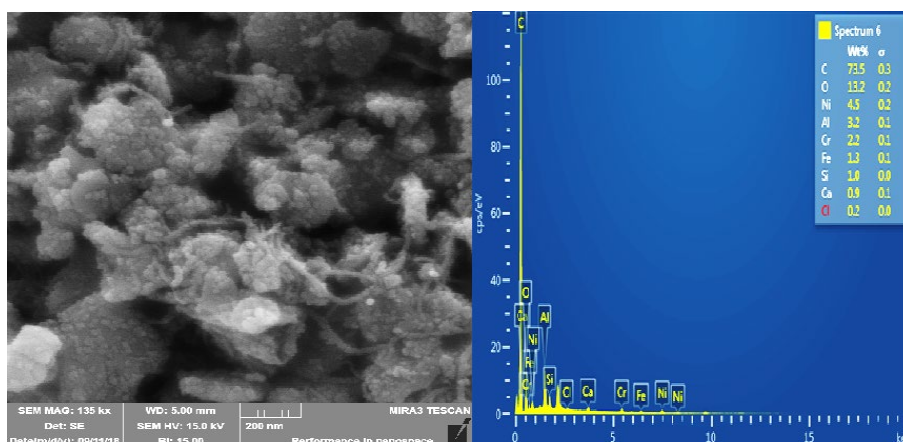


Fig 9. SEM images and EDS analysis of the prepared F-MWCNTs/ Cr₂O₃-NiO (1:0.5) g nanocomposites

Photocatalytic Activity of the Nanocomposite

Effect of the amount of nanocomposite on photocatalytic removal of BBG dye over nanocomposite

The obtained results of photocatalytic removal of BBG dye over nanocomposite under using different masses of the used composite are presented in Fig. 10. These used masses were as follows, 0.006, 0.01, 0.03, and 0.05 g. In each case, a required mass of the composite was suspended in 30 mL of dye aqueous solution (50 ppm) under irradiation with UV light at 298 K. All experiments were carried out for 60 min. From the obtained results, it was found that there was an increase in the efficiency of dye removal with an increase in the amount of the used composite. The higher efficiency of dye removal was achieved at mass equal to 0.03 g. After that, the increase in nanocomposite weight to 0.05 g leads to the reduction in efficiency of dye removal. At high concentrations of the nanocomposite upon using a same light source, the nanoparticles of MWCNTs/Cr₂O₃-NiO can form inner filter inside reaction mixture which leads to absorb the photons and prevent crossing passing them into the other side of the reaction mixture. This leads to reducing the number of excited particles, which results in a reduction in the formation of redox species including conduction band electrons and valence band holes. These redox species play a significant role in redox reaction at the

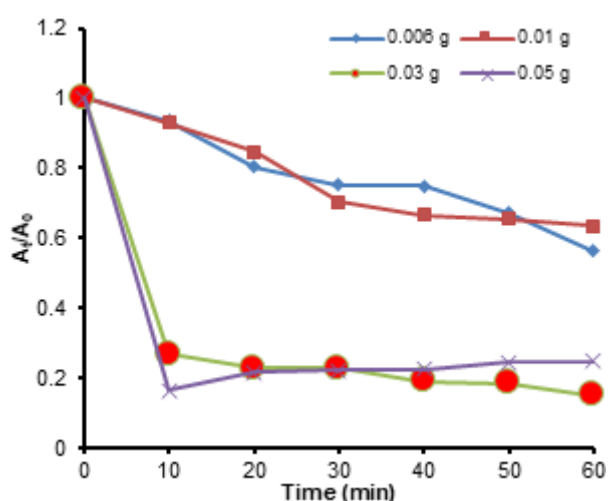


Fig 10. Effect of the amount of nanocomposite on BBG dye removal over different masses of the composites

surface of the used catalyst, which leads to a reduction in the efficiency of dye removal [35].

Effect of pH on photocatalytic BBG dye removal over MWCNT/Cr₂O₃-NiO

To investigate the effect of pH of the reaction mixture on the efficiency of BBG dye removal over prepared nanocomposite. A series of experiments were performed at different pHs values under constant other reaction parameters. For each case, 0.03 g of the nanocomposite was suspended in 30 mL of aqueous BBG dye solution 50 ppm under UV light at 298 K for 60 min. The obtained results of this part are presented in Fig. 11. From these results, the best result of removal efficiency was obtained at pH = 5 and in this case, the efficiency of dye removal was around 93.68%. Then after this value, any increase in the pH values up to 9 leads to a decrease in the removal efficiency. This can be resulted due to the repulsion between the negatively charged surface and the anionic groups in dye molecules [36-37].

Effect of temperature on photocatalytic removal of BBG over nanocomposite

The effect of reaction temperature on the efficiency of photocatalytic removal of BBG dye over nanocomposite was investigated by performing the reactions under different temperatures in the range from

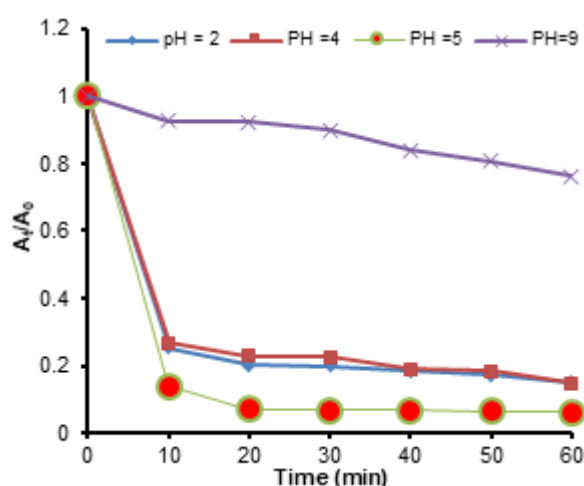


Fig 11. Effect of pHs of dye solution on the removal efficiency of BBG over nanocomposite

283–308 K with increasing by five degrees for each increment. Other reaction conditions were kept constant. These conditions involve using a dye in a concentration of 50 ppm in 30 mL, nanocomposite loading of 0.03 g, and the pH of the reaction mixture was kept at 5. The obtained results are shown in Fig. 12, and from these results, it was found that the efficiency of dye removal was enhanced with increasing temperature of the reaction mixture and the best removal efficiency was recorded at 303 K, and it was around 99.8%. This observation can be attributed to the formation of a high concentration of free radicals upon elevation in reaction temperature. These active species would contribute to the removal of dye molecules. Besides that, an increase in temperature leads to an increase of diffusion rate of dye molecules from the bulk solution to be adsorbed at the active sites on the surface. At higher temperatures, greater than 303 K, any increase in reaction temperature can affect the amount of adsorbed molecules at the surface and increase the rate of desorption of dye molecules away from the surface. This effect leads to reduce the efficiency of dye removal under these conditions [38].

Adsorption Isotherms

The results of the adsorption of BBG dye over nanocomposites are shown in Fig. 13 and 14, and Table 3. In this part, both Langmuir and Freundlich adsorption isotherm models were investigated for adsorption of BBG over nanocomposite.

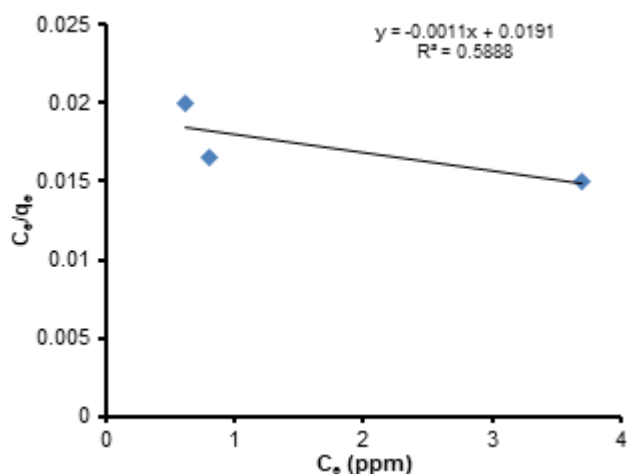


Fig 13. Langmuir adsorption isotherm for the adsorption of BBG over nanocomposite

From the presented results in Table 3, the value of the correction factor (R^2) to Langmuir is lower than the value of the correction coefficient (R^2) for Freundlich, but the number of adsorbed layers is 0.899. In this case, the formation of a single monolayer of adsorbate on the surface agrees on with the Langmuir adsorption model which make the adsorption seems to be more fitted with Langmuir adsorption isotherm. [39].

Kinetics of Adsorption of BBG over Nanocomposite

Kinetics study for adsorption of BBG dye over nanocomposite was investigated, and the obtained results are presented in Table 4 and Fig. 15 and 16. From

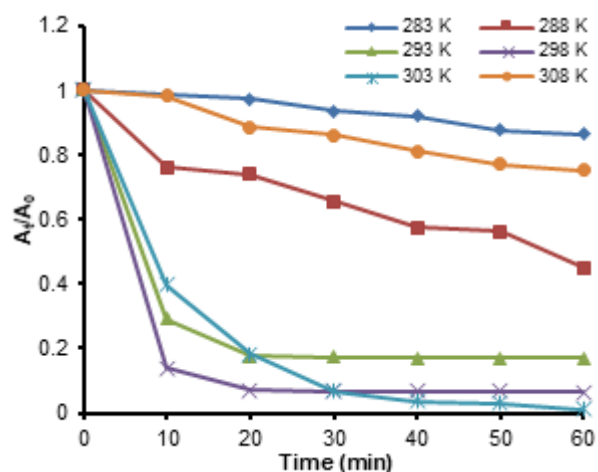


Fig 12. Effect of temperature on removal efficiency of BBG over nanocomposite

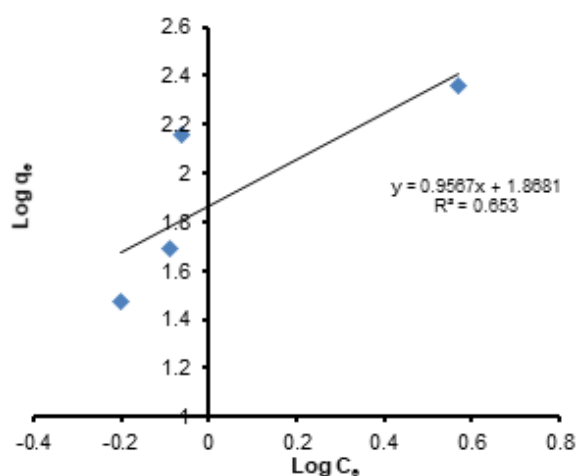


Fig 14. Freundlich adsorption isotherm for adsorption of BBG over the used nanocomposite

the obtained results, it was found that the value of the correction factor for the pseudo-first-order kinetic model was ranged from 0.8493 to 1.000. It was lower than the values of the pseudo-second-order kinetic model, which was ranged from 0.9987 to 1.000. From these results, it is clear that adsorption of BBG dye over nanocomposite was more fitted with a pseudo-second-order kinetic model.

The pseudo-first order kinetic model is given by Lagergren [39]

$$\ln(q_t - q_e) = \ln(q_e) - k_1 t \quad (2)$$

where q_e and q_t (mg/g) are the amounts of the BBG adsorbed at equilibrium and at time t (min), respectively, and k_1 (min^{-1}) is the adsorption rate constant. The pseudo-second-order kinetic model is given by the following equation:

$$\frac{t}{q_t} = \frac{1}{k_2 q_e^2} + \frac{t}{q_e} \quad (3)$$

where k_2 (g/mg min) is the rate constant of the second-order equation.

Table 3. Langmuir and Freundlich adsorption isotherms constants for adsorption of BBG over the used nanocomposite

Isotherms	Parameters	Values
Freundlich	K_F	5.682
	N	0.899
	R^2	0.9887
Langmuir	Q_m	909.09
	K_L	0.0576
	R^2	0.5888

Table 4. The adsorption parameters for BBG adsorption onto FMWCNTs/Cr₂O₃-NiO

Weight (g)	Pseudo-first-order model			
	q_e , exp (mg/g)	q_e , cal (mg/g)	K_1 (min^{-1})	R^2
0.006	231.3	64.32	0.1043	0.8553
0.01	147.39	10.41	0.0586	0.9611
0.03	49.18	2.57	0.0379	0.8493
0.05	29.62	34.12	0.0938	1
	Pseudo-second-order model			
	q_e , exp (mg/g)	q_e , cal (mg/g)	K_2 (g/mg min)	R^2
0.006	231.3	283.09	0.0026	0.9987
0.01	147.39	147.05	0.028	1
0.03	49.18	49.5	0.05	0.9998
0.05	29.62	29.67	0.151	0.9999

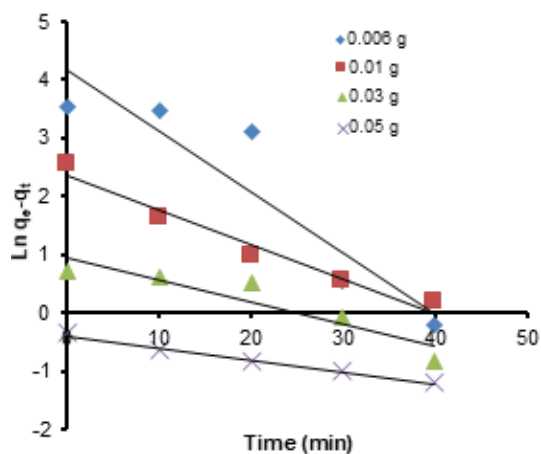


Fig 15. The pseudo-first-order onto FMWCNTs/Cr₂O₃-NiO for BBG adsorption

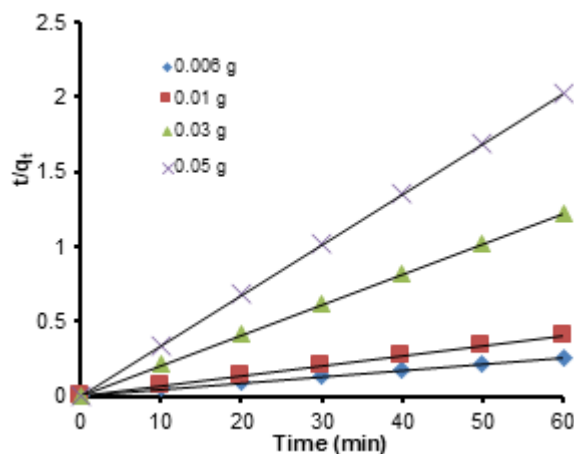


Fig 16. Pseudo-second order kinetic model over FMWCNT/ Cr₂O₃-NiO

■ CONCLUSION

The adsorption and photocatalytic removal of BBG dye over nanocomposite depend on the dosage of the nanocomposite, pH value, and reaction temperature. The complete photocatalytic removal of BBG dye was investigated by using F-MWCNT/MO under UV illumination. The optimal conditions of removal dye were found to be at pH of 5, nanocomposite dosage of 0.03 g/L, the temperature of 303 K with 50 ppm of the dye solution and illumination time of 60 min. From the obtained results of equilibrium, adsorption isotherm refers to the formation of monolayer adsorption, and hence it was more fitted with the Langmuir adsorption model. The adsorption process of BBG dye over the prepared nanocomposite was fitted with the pseudo-second-order kinetic model.

■ ACKNOWLEDGMENTS

The authors would like to thank Babylon University, College of Science in Iraq for funding this work as a part of an annual research plan for academic staff.

■ REFERENCES

- [1] Xu, A.Z., Yang, M.S., Wu, Q., Hu, X.M., and Jiang, L., 2005, Flow field induced steady alignment of oxidized multi-walled carbon nanotubes, *Chin. Chem. Lett.*, 16 (6), 849–852.
- [2] Iijima, S., and Ichihashi, T., 1993, Single-shell carbon nanotubes of 1-nm diameter, *Nature*, 363, 603–605.
- [3] Iijima, S., 1991, Helical microtubules of graphitic carbon, *Nature*, 354 (7), 56–58.
- [4] Wepasnick, K.A., Smith, B.A., Bitter, J.L., and Fairbrother, D.H., 2010, Chemical and structural characterization of carbon nanotube surfaces, *Anal. Bioanal. Chem.*, 396 (3), 1003–1014.
- [5] Iijima, S., and Ichihashi, T., 1993, Single-shell carbon nanotubes of 1-nm diameter, *Nature*, 363, 603–605.
- [6] Jishi, R.A., Venkataraman, L., Dresselhaus, M.S., and Dresselhaus, G., 1993, Phonon modes in carbon nanotubules, *Chem. Phys. Lett.*, 209 (1-2), 77–82.
- [7] Wang, N., Tang, Z.K., Li, G.D., and Chen, J.S., 2000, Materials science: Single walled 4Å carbon nanotube arrays, *Nature*, 408 (6808), 50–51.
- [8] Liu, X., Huber, T.A., Kopac, M.C., and Pickup, P.G., 2009, Ru oxide/carbon nanotube composites for supercapacitors prepared by spontaneous reduction of Ru(VI) and Ru(VII), *Electrochim. Acta*, 54 (27), 7141–7147.
- [9] Leonov, A.A., Khasanov, A.O., Danchenko, V.A., and Khasanov, O.L., 2017, Spark plasma sintering of ceramic matrix composite based on alumina, reinforced by carbon nanotubes, *IOP Conf. Ser.: Mater. Sci. Eng.*, 286, 012034.
- [10] Keshri, A.K., Huang, J., Singh, V., Choi, W., Seal, S., and Agarwal, A., 2010, Synthesis of aluminum oxide coating with carbon nanotube reinforcement produced by chemical vapor deposition for improved fracture and wear resistance, *Carbon*, 48 (2), 431–442.
- [11] Bandow, S., Asaka, S., Saito, Y., Rao, A.M., Grigorian, L., Richter, E., and Eklund, P.C., 1998, Importance of transmission electron microscopy for carbon nanomaterials, *Phys. Rev. Lett.*, 80 (17), 3779–3782.
- [12] Koval'chuk, A.A., Shevchenko, V.G., Shchegolikhin, A.N., Nedorezova, P.M., Klyamkina, A.N., and Aladyshev, A.M., 2008, Effect of carbon nanotube functionalization on the structural and mechanical properties of polypropylene/MWCNT composites, *Macromolecules*, 41 (20), 7536–7542.
- [13] Amiri, A., Maghrebi, M., Baniadam, M., and Zeinali Heris, S.Z., 2011, One-pot, efficient functionalization of multi-walled carbon nanotubes with diamines by microwave method, *Appl. Surf. Sci.*, 257 (23), 10261–10266.
- [14] Cuentas-Gallegos, A.K., Martínez-Rosales, R., Rincón, M.E., Hirata, G.A., and Orozco, G., 2006, Design of hybrid materials based on carbon nanotubes and polyoxometalates, *Opt. Mater.*, 29 (1), 126–133.
- [15] Hojati-Talemi, P., and Simon, G., 2009, Microwave-based treatments for multi-walled carbon nanotubes, *Phys. Status Solidi C*, 6 (10), 2170–2173.
- [16] Smith, B., Wepasnick, K., Schrote, K.E., Cho, H.H., Ball, W.P., and Fairbrother, D.H., 2009, Influence of surface oxides on the colloidal stability of multi-

- walled carbon nanotubes: A structure-property relationship, *Langmuir*, 25 (17), 9767–9776.
- [17] Lu, C., and Chiu, H., 2008, Chemical modification of multiwalled carbon nanotubes for sorption of Zn^{2+} from aqueous solution, *Chem. Eng. J.*, 139 (3), 462–468.
- [18] Morales-Lara, F., Pérez-Mendoza, M.J., Altmajer-Vaz, D., García-Román, M., Melguizo, M., López-Garzón, F.J., and Domingo-García, M., 2013, Functionalization of multiwall carbon nanotubes by ozone at basic pH. Comparison with oxygen plasma and ozone in gas phase, *J. Phys. Chem. C*, 117 (22), 11647–11655.
- [19] Eder, D., 2010, Carbon nanotube–inorganic hybrids, *Chem. Rev.*, 110 (3), 1348–1385.
- [20] Fu, K., Huang, W., Lin, Y., Riddle, L.A., Carroll, D.L., and Sun, Y.P., 2001, Defunctionalization of functionalized carbon nanotubes, *Nano Lett.*, 1 (8), 439–441.
- [21] Sun, Y., Wilson, S.R., and Schuster, D.I., 2001, High dissolution and strong light emission of carbon nanotubes in aromatic amine solvents, *J. Am. Chem. Soc.*, 123 (22), 5348–5349.
- [22] Gupta, V.K., Agarwal, S., and Saleh, T.A., 2011, Synthesis and characterization of alumina-coated carbon nanotubes and their application for lead removal, *J. Hazard. Mater.*, 185 (1), 17–23.
- [23] Wang, S., Shi, X., Shao, G., Duan, X., Yang, H., and Wang, T., 2008, Preparation, characterization and photocatalytic activity of multi-walled carbon nanotube-supported tungsten trioxide composites, *J. Phys. Chem. Solids*, 69 (10), 2396–2400.
- [24] Mitróová, Z., Tomašovičová, N., Lancz, G., Kováč, J., Vávra, I., and Kopčanský, P., 2010, Preparation and characterization of carbon nanotubes functionalized by magnetite nanoparticles, *Proceeding of the 2nd NANOCON International Conference*, Olomouc, Czech Republic, 12–14 October 2010.
- [25] Xu, Y.J., Zhuang, Y., and Fu, X., 2010, New insight for the enhanced photocatalytic activity of TiO_2 by doping carbon nanotubes: A case study on degradation of benzene and methyl orange, *J. Phys. Chem. C*, 114 (6), 2669–2676.
- [26] Yu, Y., Yu, J.C., Yu, J.G., Kwok, Y.C., Che, Y.K., Zhao, J.C., Ding, L., Ge, W.K., and Wong, P.K., 2005, Enhancement of photocatalytic activity of mesoporous TiO_2 by using carbon nanotubes, *Appl. Catal., A*, 289 (2), 186–196.
- [27] Yudasaka, M., Kikuchi, R., Matsui, T., Ohki, Y., Yoshimura, S., and Ota, E., 1995, Specific conditions for Ni catalyzed carbon nanotube growth by chemical vapor deposition, *Appl. Phys. Lett.*, 67 (17), 2477–2479.
- [28] Yukasaka, M., Kikuchi, R., Ohki, Y., Ota, E., and Yoshimura, S., 1997, Behavior of Ni in carbon nanotube nucleation, *Appl. Phys. Lett.*, 70 (14), 1817–1818.
- [29] Skoog, D.A., Holler, F.J., and Crouch, S.R., 2007, Principles of Instrumental Analysis, Principles of Instrumental Analysis, 6th Ed., Thomson Brooks/Cole, Belmont, CA, USA.
- [30] Wu, X., Hong, X., Luo, Z., Hui, K.S., Chen, H., Wu, J., Hui, K.N. Li, L., Nan, J., and Zang, Q., 2013, The effects of surface modification on the supercapacitive behaviors of novel mesoporous carbon derived from rod-like hydroxyapatite template, *Electrochim. Acta*, 89, 400–406.
- [31] Pilehvar, S., Rather, J.A., Dardenne, F., Robbens, J., Blust, R., and De Wael, K., 2013, Carbon nanotubes based electrochemical detection of hydroxylated polychlorinated biphenyl in human blood aptasensing platform for the serum, *Biosens. Bioelectron.*, 54, 78–84.
- [32] Fadaei, S., Moghadam, F.N., Hashemi, M., and Pourzamani, H., 2017, BTEX removal from aqueous solution by modified multi-walled carbon nanotubes with ozone, *Anuário IGEO*, 40 (1), 235–242.
- [33] Yildirim, A., and Seçkin, T., 2014, *In situ* preparation of polyether amine functionalized MWCNT nanofiller as reinforcing agents, *Adv. Mat. Sci. Eng.*, 2014, 356920.
- [34] Kim, S.K., and Park, H.S., 2014, Multiwalled carbon nanotubes coated with a thin carbon layer for use as composite electrodes in supercapacitors, *RSC Adv.*, 4 (88), 47827–47832.
- [35] Hayat, K., Gondal, M.A., Khaled, M.M., and Ahmed, S., 2010, Kinetic study of laser-induced photocatalytic degradation of dye (alizarin yellow)

- from wastewater using nanostructured ZnO, *J. Environ. Sci. Health., Part A Toxic/Hazard. Subst. Environ. Eng.*, 45 (11), 1413–1420.
- [36] Mohammad, E.J., Lafta, A.J., and Kahdim, S.H., 2016, Photocatalytic removal of reactive yellow 145 dye from simulated textile wastewaters over supported (Co, Ni)₃O₄/Al₂O₃ co-catalyst, *Pol. J. Chem. Technol.*, 18 (3), 1–9.
- [37] Mohammad, E.J., Kareem, M.M., and Atiyah, A.J., 2018, Removal of dye Bismarck brown G by photocatalytic reaction over prepared co-oxide Cr₂O₃-NiO: A kinetic study, *Asian J. Chem.*, 30 (11), 2527–2532.
- [38] Soares, E.T., Lansarin, M.A., and Moro, C.C., 2007, A study of process variables for the photocatalytic degradation of rhodamine B, *Braz. J. Chem. Eng.*, 24 (1), 29–36.
- [39] Lagergren, S., 1898, About the theory of so-called adsorption of soluble substances, *K. Sven. Vetensk.Akad. Handl.*, 24 (4), 1–39.